Science of the Total Environment 715 (2020) 136920

Contents lists available at ScienceDirect

Science of the Total Environment

journal homepage: www.elsevier.com/locate/scitotenv

Methane and nitrous oxide porewater concentrations and surface fluxes of a regulated river

Jorge A. Villa [a,b,*], Garrett J. Smith [c], Yang Ju [a], Lupita Renteria [d], Jordan C. Angle [c], Evan Arntzen [d], Samuel F. Harding [d], Huiying Ren [d], Xingyuan Chen [d], Audrey H. Sawyer [e], Emily B. Graham [d], James C. Stegen [d], Kelly C. Wrighton [f], Gil Bohrer [a]

[a] Department of Civil, Environmental and Geodetic Engineering, Ohio State University, 470 Hitchcock Hall, 2070 Neil Avenue, Columbus, OH 43210, USA
[b] School of Geosciences, University of Louisiana at Lafayette, 323 Hamilton Hall, 611 McKinely Street, Lafayette, LA 70504, USA
[c] Department of Microbiology, Ohio State University, 105 Biological Sciences Building, 484 W. 12 Ave., Columbus, OH 43210, USA
[d] Pacific National Northwest Laboratory, 902 Battelle Blvd, Richland, WA 99354, USA
[e] School of Earth Sciences, Ohio State University, 125 Oval Dr S, Columbus, OH 43210, USA
[f] Department of Soil and Crop Sciences, Colorado State University, 307 University Ave, Fort Collins, CO 80521, USA

HIGHLIGHTS

- A better understanding of methane and nitrous oxide emissions from rivers is needed.
- Porewater concentrations and fluxes were measured at three different hydrological stages.
- We used co-located peepers and static chambers at a beach transect in three elevations.
- River stage forced different gas dynamics in vertical and horizontal planes.
- Small-scale hydro-biogeochemical exchanges are crucial for better predictions.

GRAPHICAL ABSTRACT

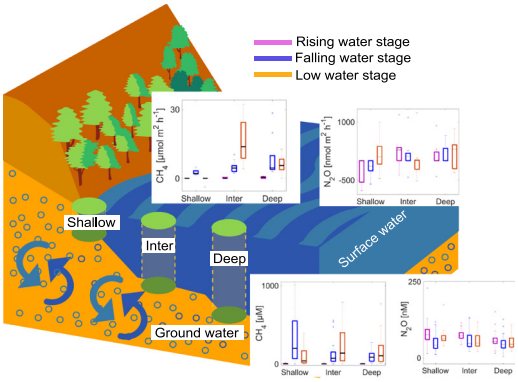

ARTICLE INFO

Article history:
Received 22 November 2019
Received in revised form 22 January 2020
Accepted 23 January 2020
Available online 27 January 2020

Editor: José Virgílio Cruz

Keywords:
Hyporheic zone
Methane conductance
Porewater
Methane flux
Nitrous oxide flux

ABSTRACT

Greenhouse gas (GHG) emissions from rivers are a critical missing component of current global GHG models. Their exclusion is mainly due to a lack of in-situ measurements and a poor understanding of the spatiotemporal dynamics of GHG production and emissions, which prevents optimal model parametrization. We combined simultaneous observations of porewater concentrations along different beach positions and depths, and surface fluxes of methane and nitrous oxide at a plot scale in a large regulated river during three water stages: rising, falling, and low. Our goal was to gain insights into the interactions between hydrological exchanges and GHG emissions and elucidate possible hypotheses that could guide future research on the mechanisms of GHG production, consumption, and transport in the hyporheic zone (HZ). Results indicate that the site functioned as a net source of methane. Surface fluxes of methane during river water stages at three beach positions (shallow, intermediate and deep) correlated with porewater concentrations of methane. However, fluxes were significantly higher in the intermediate position during the low water stage, suggesting that low residence time increased methane emissions. Vertical profiles of methane peaked at different depths, indicating an influence of the magnitude

* Corresponding author at: School of Geosciences, University of Louisiana at Lafayette, 323 Hamilton Hall, 611 McKinley Street, Lafayette, LA 70504, USA.
E-mail address: jorge.villa@louisiana.edu (J.A. Villa).

https://doi.org/10.1016/j.scitotenv.2020.136920
0048-9697/

and direction of the hyporheic mixing during the different river water stages on methane production and consumption. The site acted as either a sink or a source of nitrous oxide depending on the elevation of the water column. Nitrous oxide porewater concentrations peaked at the upper layers of the sediment throughout the different water stages. River hydrological stages significantly influenced porewater concentrations and fluxes of GHG, probably by influencing heterotrophic respiration (production and consumption processes) and transport to and from the HZ. Our results highlight the importance of including dynamic hydrological exchanges when studying and modeling GHG production and consumption in the HZ of large rivers.

1. Introduction

Rivers and streams cover a relatively small area of the planet's terrestrial phase (0.47%). Nonetheless, they play a pivotal role in greenhouse gas (GHG) emissions (Raymond et al., 2013). It is estimated that they emit annually 6.6 Pg of carbon dioxide (CO_2) (Raymond et al., 2013), 26.8 Tg of methane (CH_4) (Stanley et al., 2016) and 1.1 Tg of nitrous oxide (N_2O) (Beaulieu et al., 2011). In other words, this is the equivalent to ~12% of CO_2 emissions from fossil fuels and industry (Jackson et al., 2017), and ~5% and ~10% of global methane and N_2O emissions, respectively (Beaulieu et al., 2011; Saunois et al., 2016). The disproportionate contributions from rivers to GHG budgets have challenged the early assumption of rivers as "passive" or "neutral" pipes in global and regional GHG budgets (Cole et al., 2007; Aufdenkampe et al., 2011), placing them as active hotspots for GHG exchange.

Whereas the biogeochemical processes that lead to CO_2 emissions from rivers have traditionally received more attention (Raymond et al., 2013; Hotchkiss et al., 2015) and are relatively better represented in current models (e.g., E3SM, Golaz et al., 2019), the processes that lead to methane and N_2O emissions remain poorly constrained in space and time (Bridgham et al., 2013; Quick et al., 2019). Methane and N_2O emissions are low compared with those of CO_2, yet on an equal mass basis, they have 45 and 270 times the potential of CO_2 to warm the atmosphere over a 100-year horizon, respectively (Neubauer and Megonigal, 2015). Most of the biogeochemical activity that leads to methane and N_2O production and consequent emission in rivers occurs within the hyporheic zone (HZ), a transition zone in the saturated sediments adjacent to the streamflow where surface water and subsurface waters are permanently mixing (McClain et al., 2003; Krause et al., 2011). The mixing of downwelling oxidized surface water, and upwelling of reduced subsurface water provides a unique environment of enhanced nutrient and light availability, gradients of temperature and redox potentials, pH, organic matter content, and microbial numbers and activity (Woessner, 2017). This environment represent biogeochemical hotspots for microbial activity where aerobic and anaerobic microbial metabolisms co-occur (Boulton et al., 1998). In general, the HZ is a net source of methane and N_2O (Reeder et al., 2018).

Hydrologic exchange strongly affects the flow of organic dissolved carbon, an essential microbial substrate for GHG production processes, as well as the transport of GHG themselves. Methane can be produced in the anaerobic environment within the HZ from CO_2 and H_2 or acetate during the degradation of organic matter (Lyu et al., 2018). Methane may also be transported from the surrounding upland areas dissolved in groundwater (Jones and Mulholland, 1998). Once in the HZ, methane can be oxidized and transformed back into CO_2 with sufficient electron acceptors, particularly oxygen, by methanotrophic microorganisms (Chistoserdova et al., 2009). The remaining portion of methane that is not oxidized can be emitted via diffusion, ebullition, or plant-mediated transport (Bridgham et al., 2013).

N_2O production in the HZ is mainly the result of four distinct processes: (1) denitrification or reduction of nitrate or nitrite to dinitrogen with nitrous oxide as an intermediate, (2) by-products of oxidation of ammonia to nitrate or nitrite, (3) dissimilatory reduction of nitrate to ammonia, and (4) chemo-denitrification involving the abiotic reaction of nitrite with iron(II) (Quick et al., 2019), of which denitrification is thought as the main production pathway in lotic systems (Baulch et al., 2011a; Beaulieu et al., 2011). N_2O transport from the HZ to the atmosphere occurs primarily via diffusion (Baulch et al., 2011a).

A better understanding of the dynamics and interactions of different processes throughout the HZ is needed in order to resolve the role of rivers in global GHG emissions correctly. There is a need for an improved mechanistic understanding of the biogeochemical processes involved in the production, consumption, and transformation of carbon and nitrogen species leading to riverine GHG emissions. However, river systems are spatially complex and temporally dynamic, making predictions of GHG emissions, especially challenging. The lack of observations for evaluating specific parameters that describe each process often leads to simplistic representation in models, and consequently, high sensitivity and uncertainty in the model results. The inclusion of sub-models that can resolve transient hydrological exchanges in land-surface models is paramount to more robustly represent biogeochemical processes in the terrestrial-aquatic interphases (Buchkowski et al., 2017; Graham et al., 2019). With very few exceptions (e.g., Rulík et al., 2000; Bednařík et al., 2015; Comer-Warner et al., 2018), field studies of GHG fluxes in rivers rarely address small-scale spatial variability across the bank, and temporal variation in relation to the hydrological dynamics between the groundwater and river. In addition, very few have considered simultaneously methane and N_2O and how they may be linked at the site scale.

Here we present results from methane and N_2O porewater concentrations and chamber flux measurements conducted at different river stages at a plot of the Columbia River, a large regulated river. Our goal was to assess the spatio-temporal variability in porewater concentrations and surface fluxes. We further utilize the results to identify the relationships between HZ hydrological processes and the sources or sinks of methane and N_2O.

2. Methods

2.1. Study site and sampling approach

This study was conducted in the experimental 'Genome to Greenhouse Gas (3G) observatory' at the Columbia River on the Hanford Reach (Hanford 300 Area), Washington State, USA (Fig. 1). The observatory consists of an array of 3 triplicate porewater samplers (peepers) deployed at a sandy beach on bank-to-river transects (6 m long) along a microtopographic gradient representing three nominal beach positions: shallow, intermediate and deep (Fig. 1B). The sampling array encompasses a small, 11 m-long plot. The plot is located in a small cove that isolates the site from the flow influences of the main river channel. Concurrent measurements of methane, CO_2 and N_2O porewater concentrations and surface fluxes of methane and N_2O were conducted during three distinct river stages representing the main phases of a typical hydrological year at the study site, ~80 km downstream of the Priest Rapids Dam at the Hanford Reach. We sampled on three occasions between 25th April and 25th August in 2018 consisting of (1) a rising water stage during spring snowmelt, (2) a falling water stage during summer after the annual peak in early June, and (3) a highly regulated

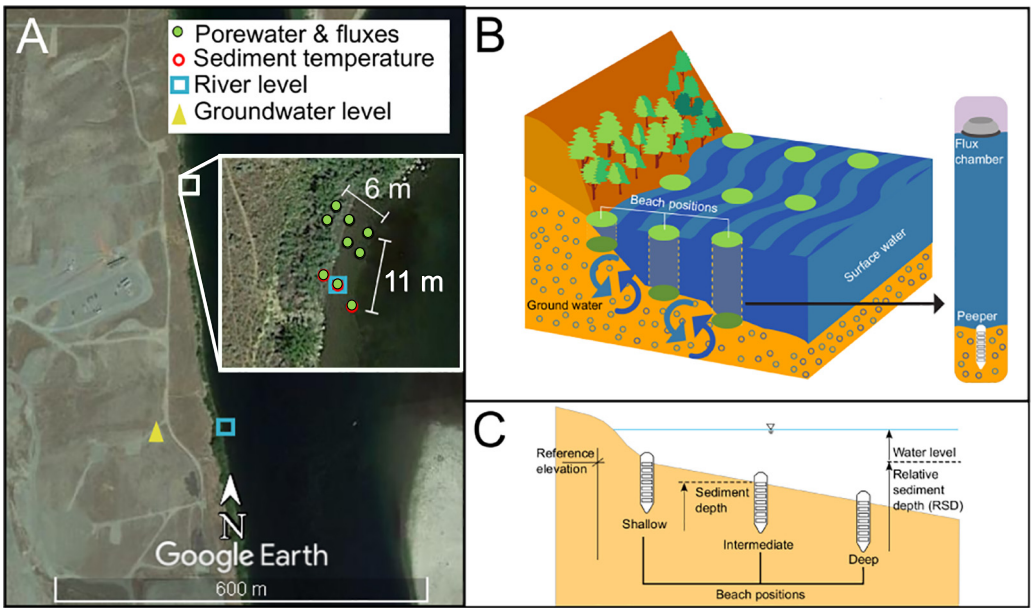

Fig. 1. Experimental design. (A) Peeper array at the 3G observatory and river and groundwater monitoring at the 300 Area, Hanford reach, Washington State. (B) Diagram depicting the general sampling design and (C) the conventions used throughout the manuscript. The transect marked in red in (A) denotes the transect where sediment temperatures were measured. (For interpretation of the references to color in this figure legend, the reader is referred to the web version of this article.)

low water stage starting late in the summer that typically extends to the onset of the next spring snowmelt.

2.2. River levels and hydraulic gradient

River water and groundwater levels were recorded using pressure transducers. We conducted river water measurements at the 3G observatory during August 2018 (5 min resolution) and river water and groundwater measurements in a transect perpendicular to the river, 410 m downstream of the 3G observatory during 2018 (15 min resolution) (Fig. 1A). We generated a time series for the 3G observatory during 2018 using water levels from the point of measurement downstream ($r^2 = 0.99$, $p < 0{,}001$, 27 days in August), and a known discrete level at the 3G site. We used as a zero-reference location for the water level the sediment surface of the shallow position (Fig. 1C).

To determine the strength of groundwater flow toward the river, we calculated the hydraulic gradient (*HG*, m m^{-1}) between the river water and groundwater-well level as:

$$HG = \Delta h\, L^{-1} \quad (1)$$

where Δh is the head difference between the river water level (m) and the groundwater level of the well (m) at a given time, and L is the distance between their two points of measurement (114 m). Sediment temperatures (at 10 cm sediment depth) were measured at each position along one transect during the study period using thermistors (marked in red in Fig. 1A).

2.3. Porewater sampling and processing

Vertical profiles of methane, N_2O, and CO_2 concentration of sediment porewater were determined at each gradient's position using the peepers described by MacDonald et al. (2013). The peepers allowed for non-destructive consecutive sampling of the sediment profile at the same depth and beach positions. The peepers feature 20 stacked cells (61.4 ml) at a 2.8 cm vertical resolution. Each cell has 22.5 cm^2 windows covered with a 0.22-μm pore size polyethersulfon membrane that allows water inside the cell to equilibrate with dissolved gas concentrations in the sediments. Cells were fitted with two sampling ports consisting of plastic tubing that allowed water extraction and refill. We used standard 4-in. PCV conduit anchored to the river sediments above the peeper location with rebar to house the peeper tubing, allowing for easy sampling even when water levels were high, and marking the peeper location. Peepers were deployed two months before our first sampling to ensure equilibration, which usually could take between 4 days and up to three weeks (MacDonald et al., 2013).

We sampled ten cells, starting at the top cell (at zero sediment depth) and every other after that, until reaching the bottom-most cell at 50-cm sediment depth. The sampling consisted of extracting 10-ml of water from the cells through one of the cell tubings while keeping the other connected to a container filled with N_2 to avoid oxygen intrusion that could disturb the anaerobic environment within and around the cells. After the extraction, the cell was refilled with deionized water degassed with N_2. Samples were placed in 10-ml containers pre-acidified with 0.2 ml HCl 2 M to ensure pH levels below 2.0, which prevent the post-sampling biological transformation of the gases dissolved in the sample. Then, samples were refrigerated and transported to the laboratory for further processing.

2.4. Porewater concentrations

Gas concentrations in porewater were determined using the gas chromatograph headspace equilibration technique described by (Kampbell et al., 1989). We used a 5-ml subsample of each vial to equilibrate with a 15-ml N_2 headspace. Upon equilibration, we injected 10 ml of headspace into 10-ml pre-evacuated vials and analyzed them in a gas chromatograph equipped with a flame ionization detector fitted with a 1.8 Poropack Q column and an electron capture Ni-63 detector (Shimadzu GC-2014, Shimadzu Scientific Instruments, Kyoto, Japan). Helium (25 ml min^{-1}) was used as the carrier gas for methane and CO_2 analysis and ultra-pure N_2 (10 ml min^{-1}) was used as the carrier gas for N_2O analysis. We included methane, CO_2, and N_2O check standards every 20 samples to ensure that the chromatograph maintained the calibration throughout the analysis. If the deviation between the measured value and the value of the check standard was >10%, we recalibrated the chromatograph and re-ran the samples.

Molar concentrations of methane, CO_2, and N_2O (C_{molar_pore}) were calculated from the measured gas concentrations as:

$$C_{molar\_pore} = \frac{p_i}{RT} Vh + \frac{\frac{p_i}{H^{cp}} Vl}{Vl} \quad (2)$$

where p_i is the partial pressure of methane, CO_2 or N_2O, R is the universal gas constant (m^3 Pa mol^{-1} K^{-1}), T is the room temperature (K), Vh is the volume of the headspace (ml), H^{cp} is Henry's volatility constant (m^3 Pa mol^{-1}) for methane, CO_2, and N_2O, respectively, and Vl the volume of the liquid subsample used to create the headspace (ml).

2.5. Surface flux measurements

Flux measurements were conducted using non-steady-state chambers. At each sampling, we conducted triplicate chamber measurements at the water surface right above the peepers when they were submerged or around it when the water table was below the sediments, and the peepers were surfacing. We used transparent polypropylene dome-shaped chambers (7.3×10^{-2} m^2 surface area, 7.7×10^{-3} m^3 volume), equipped with a digital thermometer to record inner temperatures and a 12v fan to mix air within the chamber and polyethylene foam in the bottom rim for flotation. For methane flux measurements, we used a single chamber connected to a cavity ring-down spectroscopy methane analyzer (Gas Scouter G4301, Picarro, Santa Clara, CA) that recirculated the air at a rate of 1 l min^{-1}. The analyzer recorded methane concentrations in the chamber at a 1-Hz frequency. Each chamber deployment lasted for 3 min, and measurements were consecutive at each peeper location.

For N_2O flux measurements, the chambers included a 30-cm long, 1.6 mm ID tube for pressure relief and a gray butyl rubber stopper as a sampling port as well. At each sampling, we deployed three chambers simultaneously for 24-minute periods at each peeper location. Six 10-ml samples were collected at 4-min frequency during each deployment, placed in pre-evacuated vials and transported for chromatography analysis in the laboratory. The concentrations of the gas samples were analyzed in the same chromatograph, and under the same quality control used to measure N_2O concentrations in porewater.

Methane and N_2O chambers positioning during sampling followed an equilateral triangular arrangement with two chambers positioned parallel to the shore. For methane sampling, we ensured the position of the single manually during the sampling period. For the N_2O sampling, we attached the cambers with polyethylene foam and then the chamber array was anchored above the peeper location by surrounding the PVC conduit used to house the peeper tubbing.

2.6. Surface flux calculations

For each methane chamber measurement, we fitted a 2 min, 1-Hz time series of methane concentrations, C_{HM} (μmol mol^{-1}), to the non-linear Hutchinson and Moiser one-dimension diffusion model (Hutchinson and Mosier, 1981; Kutzbach et al., 2007; Pedersen et al., 2010):

$$C_{HM} = C_s + (C_0 - C_s)\, e^{-kt} \quad (3)$$

where C_0 is the pre-deployment concentration of methane (μmol mol^{-1}), C_s is the constant source or sink concentration (μmol mol^{-1}), and k is a curve shape parameter (h^{-1}). C_0, C_s, and k are parameters determined by fitting the observed gas concentrations in the chamber over time, t (h). We then calculated the flux of methane (F_CH_4, μmol m^{-2} h^{-1}) at the water or sediment surface as:

$$F\_CH_4 = k\,(C_0 - C_s)\,\frac{P\,V}{R\,T\,A} \quad (4)$$

where P (Pa) is the atmospheric pressure, measured with a digital barometer at the site; V the volume of the chamber (m^3), R the universal gas constant (m^3 Pa mol^{-1} K^{-1}), T the temperature inside the chamber (K), and A the surface area of the chamber (m^2).

For N_2O chamber measurements, we calculated the molar concentrations of N_2O (C_{molar_Ch}, μmol m^{-3}), in each sample using a modified gas law, following the procedure described by (Holland et al., 1999):

$$C_{molar\_Ch} = \frac{Cv\,P}{R\,T} \quad (5)$$

where Cv is the concentration (nmol mol^{-1}) of N_2O in the sample, P is atmospheric pressure (Pa), R is the universal gas constant (m^3 Pa mol^{-1} K^{-1}), and T is the air temperature (K) of the chamber. Then, the accumulation rate, C_{rate} (nmol m^{-3} h^{-1}), was determined using the slope of the linear regression fitted to the time points (t, h) collected for each chamber after rejecting outliers in the regressions following the procedure described by (Rey-Sanchez et al., 2018):

$$C_{molar\_Ch}(t) = C_{molar\_Ch}(0) + C_{rate} \times t \quad (6)$$

and with the C_{rate}, we calculated the flux rate (F_N_2O, nmol m^{-2} h^{-1}) as:

$$F\_N_2O = \frac{V\,C_{rate}}{A} \quad (7)$$

where V is the volume of the chamber (m^3), and A the area of the water/sediment surface covered by the chamber (m^2).

We used the coefficient of determination (r^2) of the fit between the model (linear in the case of N2O or non-linear in the case of CH4) and concentration observations in the chamber and a quality control criterion. Flux measurements with $r^2 < 0.8$ were considered of poor quality and were discarded from our analyses to avoid error. Out of the 81 flux measurements for methane and N_2O, 28 for methane and 29 for N_2O, were discarded due to this criterion of poor observation quality.

2.7. Methane conductance and conductivity

We used the following general expression to solve for the bulk transfer velocity of methane, or methane conductance (K), at the different beach positions and river water stages assuming that methane is not being produced in the water column:

$$F\_CH_{4d} = K\,(C_{sed} - C_{air}\,P\,H^{cp}), for\ F > 0 \quad (8)$$

where F_CH_{4d} is methane the flux measured at each flux chamber but in units of μmol m^{-2} d^{-1} to correspond with the unit convention of conductance. C_{sed} (μmol m^{-3}) is the concentration of methane in the sediments porewater at a given depth and C_{air} (μmol m^{-3}) is the aqueous equivalent of the concentration of methane in the air, calculated as the product of the initial concentration in the chamber (μmol mol^{-1}), P the atmospheric pressure at the moment of sampling (Pa), and H^{cp} the Henry's solubility constant for methane (mol Pa^{-1} m^{-3}). The initial concentration in the chamber, representing the concentration before enclosure, was calculated as the average of the first five measurements of each chamber run.

We assume that the overall conductance, K, is the combined result of two transport processes – K_w, the conductance to methane transport in the water from the soil surface to the air, and K_s, the conductance for methane diffusion/transport in the soil from the peak concentration depth to the soil surface. Adding the resistance to methane flux in a sequential process, we obtain the term for the

combined conductance K:

$$K = \frac{K_w K_s}{K_w + K_s} \quad (9)$$

We followed the approach by Bastviken et al. (2004) to independently determine the conductance to methane in the water column K_w for each flux chamber, by solving the equation:

$$F\_CH_4 = K_w (C_{ss} - C_{air}) \quad (10)$$

where C_{ss} (μmol m^{-3}) is the concentration of methane at the surface of the sediments assumed as the concentration in the first peeper cell.

Substituting Eq. (9) into Eq. (8), and using the porewater concentration at the depth of peak concentration in the soil, C_{ps} we obtain an equation for K_s:

$$F\_CH_{4d} = \frac{K_w K_s}{K_w + K_s} (C_{ps} - C_{air}) \quad (11)$$

Eq. (11) can be solved using the value we obtained for K_w, from Eq. (10).

Then we calculated the conductivity (i.e., conductance per unit length) to methane transport/diffusion in the soil (k_s) as:

$$k_s = \frac{K_s}{D_p} \quad (12)$$

where D_p (m) is the depth at which concentration peaks in the sediment profile.

2.8. Data analysis

We processed data, fit models for flux calculations, and conducted regression tests of porewater concentrations using MATLAB ® 2018b. We used JMP Pro 14.0.0 for all other statistical tests. All the statistical tests were conducted at a 0.05 significance level.

We used Spearman rank correlation to infer the significance of the relationship between average porewater concentrations in the sediment profile and fluxes. We tested the significance of the difference of fluxes and porewater concentrations between water stages for each beach position using paired nonparametric comparisons with the Wilcoxon method. For testing the significance of the differences of water and sediment conductance and sediment conductivity between water stages and within beach positions, we used an ordinal logistic model with the conductances or the conductivity as the response variable, position as a fixed effect and water stage nested by position.

2.9. Data availability

All porewater concentrations and fluxes data will be made available through ESS-DiVE (https://ess-dive.lbl.gov/, https://doi.org/10.15485/1595105). Additional ancillary data for the Hanford site is available through the Phoenix – PNNL Environmental Information Exchange (https://www.hanford.gov/page.cfm/PHOENIX).

3. Results and discussion

3.1. Water level and sediment temperature

The water level at the shallow bank position was low (near the sediment surface) during the first part of the year until April when water levels started rising after the spring thaw (Fig. 2A). The maximum water levels (> 3 m above the reference elevation, set at the shallow

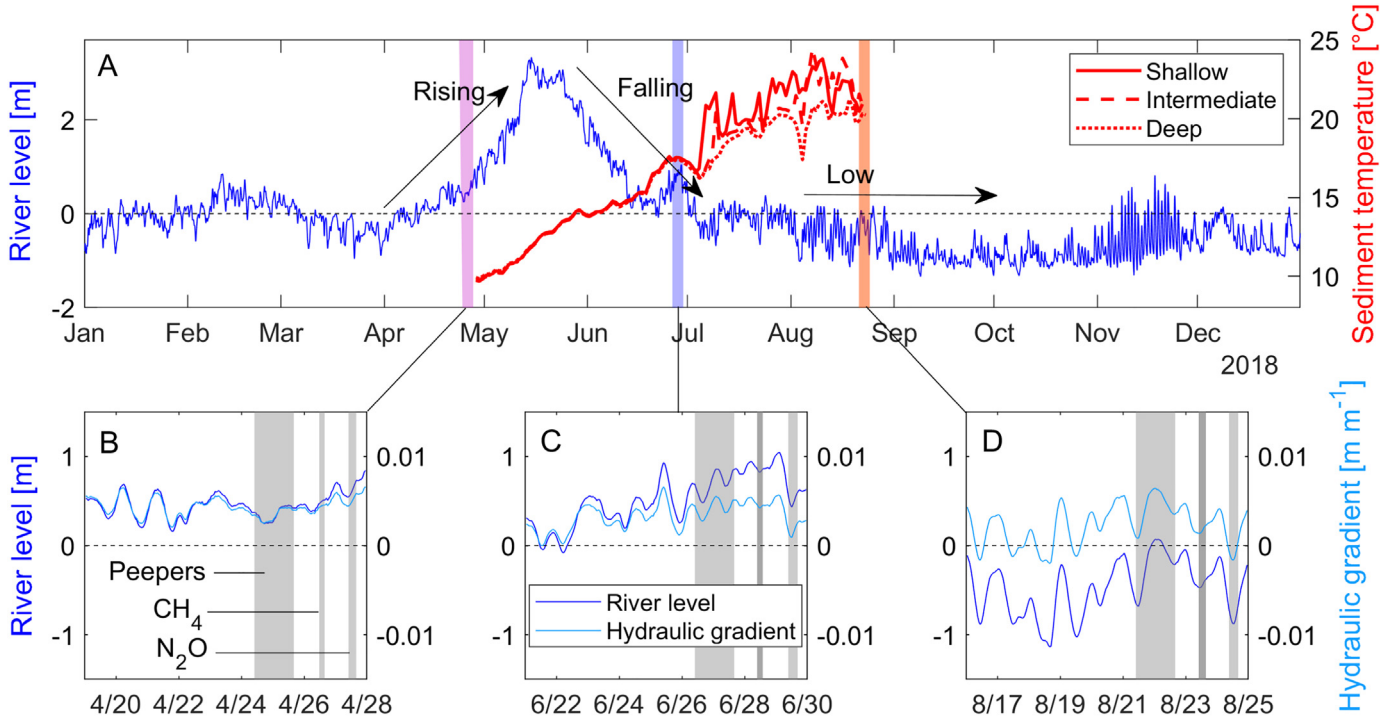

Fig. 2. Hydrological conditions during the study period (4/24 to 8/252018). (A) River water levels (dark blue), sediment temperature (red lines), and sampling periods (vertical bars with different colors). (B–D) River water levels (dark blue) and hydraulic gradient (light blue) during each river stage sampling, including the five preceding days of each sampling. The horizontal dashed line indicates the reference elevation (sediment surface at the shallow position – left axis) and the zero hydraulic gradient (right axis). Water levels above the horizontal line represent water above the sediment surface. Hydraulic gradients above that line represent river dowelling, whereas values below the line represent groundwater upwelling. At each river stage sampling, we sampled peepers first (2 days), then methane (few hours during the next day) and N_2O (few hours during the following day), as indicated by vertical gray bars (which are labeled in (B) for clarification). (For interpretation of the references to color in this figure legend, the reader is referred to the web version of this article.)

peeper position) were observed in mid-May and were followed by a steadily falling water stage until the beginning of July and remained low during the rest of the year. A brief rising limb in the second half of June was driven by dam water release during the falling stage and coincided with the moment we conducted our sampling. Water levels below the reference elevation were observed during the low stages before the rising stage and after the falling stage. The water level during the low water stage was more variable than during previous stages. The operation of the dam upstream can cause up to 0.5 m variations in water levels within a daily period (Zhou et al., 2018).

Positive hydraulic gradients (downwelling) occurred through the hydrological year, including the time during the rising and falling water stages (Fig. 2B, C). However, reversals to the negative hydraulic gradient (upwelling) were frequent during the low water stage. Hydraulic gradient reversal represents groundwater upwelling or moments when the river receives water from the aquifer. Reversals were also frequent on the days preceding the low water stage sampling (Fig. 2D).

Sediment temperature increased throughout the sampling period. In general, mean positions' temperatures had a 10 °C increase between the beginning of the study during the rising water stage in April and the study end in August (Fig. 2, Table 1). Temperatures were similar throughout the different beach positions during the rising and falling stages but differed and were more variable at the low water stage when the water level dropped below the soil surface at the reference level.

3.2. Methane porewater concentration and fluxes respond similarly to river stage variation

Methane flux to the atmosphere is the result of a balance between methane production and consumption and is influenced by the relative importance of the transport pathways, including diffusion, bubbling, and plant transport (Bridgham et al., 2013). At our site, we regard diffusion as the main transport pathway. We did not observe evidence of bubbling in our peeper chamber measurements (i.e., sudden spikes in methane concentration in the time series during chamber deployments). We also neglected the influence of plant transport because macrophyte vegetation was not present near the sampling locations, although a negligible fraction could have been transported from the shallow bank position through the vascular system of some shrubs present on the riverbank. Methane porewater concentrations and fluxes at the 3G site were negligible during the rising water stage when the sediment temperatures were low (~10 °C, Fig. 3A), which is not surprising given the high sensitivity of methane production to temperature (Yvon-Durocher et al., 2014). Methane flux was low at the shallow position during the low water stage as well, when the water level was below the sediment surface (Table 1). Despite relatively higher concentrations in the sediment profile (Fig. 3B), the water level dropdown during the low water stage may have resulted in unsaturated or oxygenated sediments and as a result, a predominantly aerobic environment that would have increased methane oxidation above the water table in the sediment column (Segers, 1998). Indeed, the porewater concentration profile at the shallow position during the low water stage showed very low concentrations throughout the sediment above the water table (Fig. 4), consistent with increased methane oxidation coupled to aerobic respiration (Conrad and Rothfuss, 1991) or low methane production due to thermodynamic exclusion (Bethke et al., 2011).

Both methane production and consumption can co-occur in sediments (Le Mer and Roger, 2001) since methanogenic and methanotrophic bacteria can be correlated in terms of population in sediments subject to flooding (Joulian et al., 1997) and the ratio between methanogens to methanotrophs is correlated to methane transfer velocity (Rey-Sanchez et al., 2019). Bednařík et al. (2015) demonstrated that benthic methane fluxes are correlated with porewater concentrations, suggesting that differences between

Table 1
Mean water levels (m) / sediment tempreature (°C) at 10-cm depth along three beach positions at the Columbia River during samplings of porewater concentrations and fluxes of methane (CH_4) and N_2O under three different river water stages. 'NA' indicates that data was not measured during that specific sampling.

Sampling	Position		
	Shallow	Intermediate	Deep
Rising water stage (porewater & fluxes)	0.46 / NA	1.00 / NA	1.44 / NA
CH_4 fluxes	0.50 / NA	1.04 / NA	1.48 / NA
N_2O fluxes	0.61 / NA	1.15 / NA	1.60 / NA
Falling water stage (porewater & fluxes)	0.78 / 17.5	1.32 / 17.5	1.76 / 17.4
CH_4 fluxes	0.83 / 17.4	1.37 / 17.4	1.82 / 17.2
N_2O fluxes	0.50 / 17.4	1.04 / 17.3	1.49 / 17.2
Low water stage (porewater & fluxes)	−0.28 / 20.9	0.26 / 21.0	0.70 / 20.1
CH_4 fluxes	0.83 / 22.4	1.37 / 21.0	1.82 / 20.1
N_2O fluxes	−0.81 / 17.4	−0.27 / 17.3	0.18 / 17.2

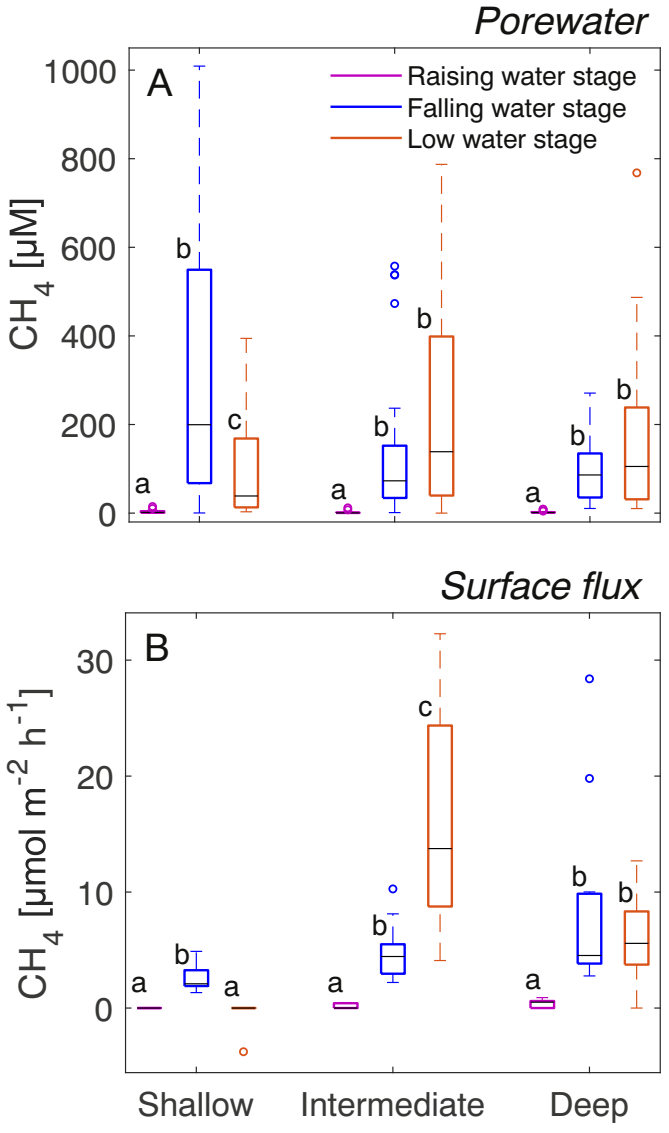

Fig. 3. (A) Integrated sediment-profile methane porewater concentrations and (B) methane fluxes along a beach transect (plot scale) at the 3G observatory during three river water stages. Boxes represent the 25th and 75th percentiles, the horizontal black line the median, circles mark outliers, defined as observations that are 1.5 greater than the upper interquartile range. Whiskers extend to the furthest observation not considered an outlier. Letters represent statistical differences calculated with non-parametric Wilcoxon paired tests for each position ($\alpha = 0.05$).

porewater concentrations and surface methane fluxes might be due to the activity of methane-oxidizing bacteria in the upper sediment layers (Oremland and Culbertson, 1992) or the water column (Matoušů et al., 2017). Although we did not systematically measure dissolved oxygen in the sediment-water interface and the water column during our samplings, we conducted a series of surveys for dissolved oxygen levels before sampling. These indicated that both the water column and the porewater at the water-sediment interface were consistently supersaturated, offering optimal conditions for biological methane oxidation. In deeper systems, such as estuaries and reservoirs, methane fluxes are greater at low water levels because of reduced storage turnover times, which is the time methane remains in the water column after being produced in the sediments (Valentine et al., 2001; Zhu et al., 2010; Lei et al., 2019). Lessened turnover times, reduce the time for potential oxidation while methane diffuses through the water column. Methane oxidation rate in the water column of rivers has been correlated with the concentration of dissolved methane in the water and with water temperature (Matoušů et al., 2018), which are proxies for the substrate and the enzymatic activity of methanotrophic microorganisms. Therefore, we hypothesize that the effect of storage-turnover time on methane oxidation will be effective in rivers, including near-bank shallow waters as well. Future studies coupling methane fluxes, and oxidation rates with simultaneous measurements of methane concentrations in the sediment and water column could help test this hypothesis.

During the falling and low water stages when sediment temperatures were more favorable for methane production, river level had a dissimilar effect on porewater concentrations and fluxes across positions, although in general, methane fluxes were correlated (Spearman's $\rho = 0.62$, $p < .001$) and followed the dynamics of the integrated sediment-profile porewater concentrations. Methane porewater concentration and fluxes decreased at the shallow position after the water level transition from the falling to the low water stage, while porewater concentration and fluxes remained similar at the deep position. In contrast, at the intermediate position, methane fluxes increased at the low stage, when the water levels were also low, while the median porewater concentration increased as well, though not at a significant level.

Low or near-zero fluxes accompanied by decreasing methane concentrations toward the surface of the sediments in the shallow position strongly indicate the activity of methanotrophs actively reducing methane emissions to the atmosphere in the upper region of the sediment profile in the shallow position during the low water stage (Fig. 4). However, the activity of methanotrophs in the upper layers of the soil profile was not evident at the intermediate or deep positions (that maintained water above the sediment surface). Even during the low water stage of the intermediate position, the peak in methane concentrations occurred well below the sediment elevation. It is possible that reduced downwelling of electron acceptors and oxygen during low water stages not only stimulated heterotrophic production of methanogenic substrates but also limited dissolved oxygen that is toxic to methanogens and reduced aerobic methanotrophic respiration. However, without specific measurements of oxidation rates at our site, it is hard to pinpoint the specific cause of the variability of methane fluxes across the different beach positions and river water stages.

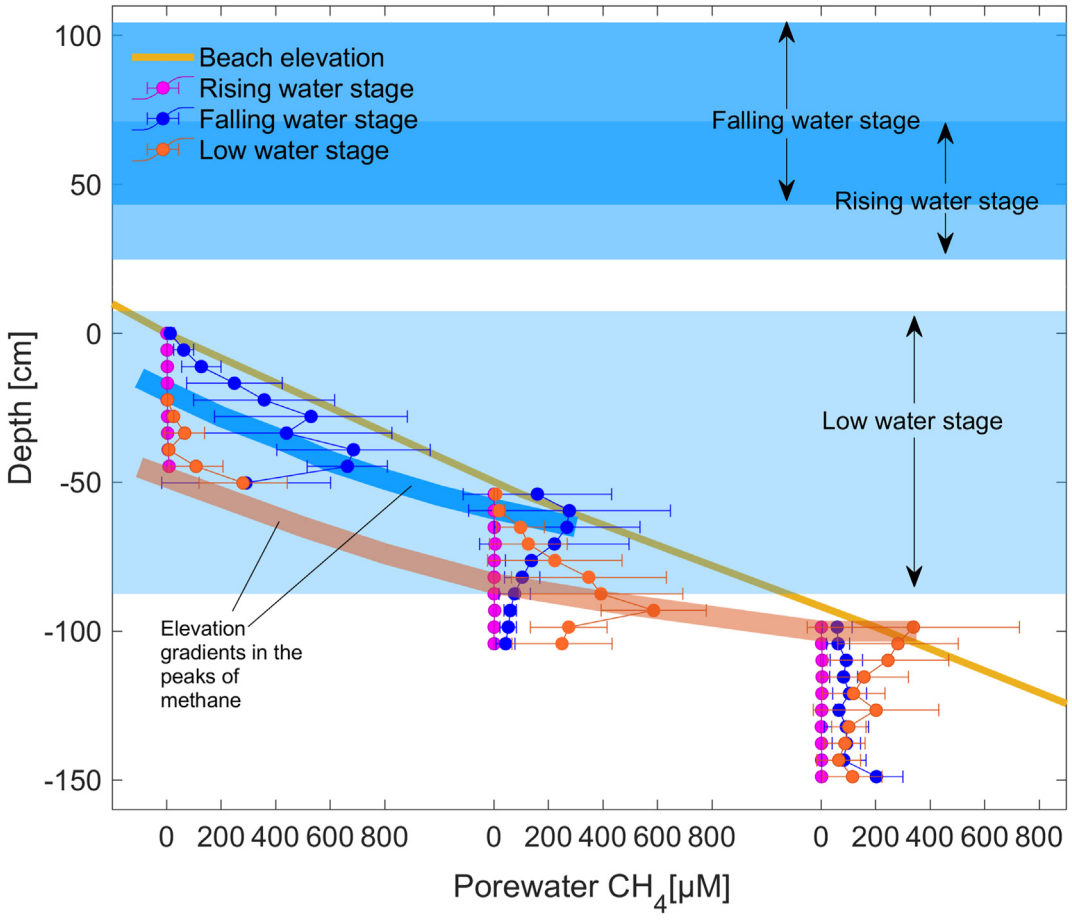

Fig. 4. Methane porewater concentrations on the sediment profile at shallow (left), intermediate (middle), and deep (right) positions of a beach transect (plot scale) at the Columbia River during three river water stages. Data points (circles) represent the mean concentration, and the error bars the standard error ($n = 3$). Horizontal blue areas indicate the water level range during the different water stages. Thick transparent color lines indicate an elevation gradient in the peaks of methane concentrations during the rising water stage (blue) and the low water stage (orange). The thick brown line represents the beach elevation along the gradient. (For interpretation of the references to color in this figure legend, the reader is referred to the web version of this article.)

Different apparent conductance to methane transport through the water column between falling and low water stages suggests that methane oxidation may occur at different rates depending on the water levels (Fig. 5A). Because we did not account for oxidation during transport in the water column, our observations of higher apparent conductance to methane transport may be the outcome of lower oxidation. Differences in conductance to methane transport through the water column were evident in the intermediate position, with larger conductance during the low water stage. In the sediment profile, conductance to methane was not different between falling and low water stages. Nonetheless, there were differences in the apparent conductance to methane in the sediments among beach positions (Fig. 5B), suggesting that there may be a significant spatial variation in oxidation rates at the plot scale.

3.3. Methane concentrations in porewater peak along an elevation gradient

Similar to surface fluxes, methane concentrations in the sediment profile are the result of a balance between methane production, consumption, and transport to and from the sediment zone. Previous studies at the Hanford Reach in similar sites to ours have shown that hydrological mixing stimulates heterotrophic respiration and organic carbon turnover (Stegen et al., 2016). Under anaerobic conditions, heterotrophic respiration at the HZ of organic matter would stimulate methane production by producing favored substrates and depleting electron acceptors (Schindler, 1998; Romeijn et al., 2019), whereas under aerobic conditions methane oxidation would be favored (Conrad and Rothfuss, 1991). Complementarily, methane may be imported in the upwelling groundwater as well. Inputs of methane dissolved in groundwater have been observed at low order streams in peat-dominated watersheds (Hope et al. 2001), headwater streams (Jones and Mulholland, 1998), streams in agricultural dominated landscapes (Comer-Warner et al., 2019) and other riverine settings including the Willamette River, the main tributary of the Columbia River (Anthony et al., 2012).

The observed methane porewater concentrations profile in the sediment showed distinct peaks that varied among bank positions following the sediment surface elevation gradient during the falling and low water stages (Fig. 4). During the falling water stage, concentrations at the shallow positions peaked at the lower sediment layers (relative sediment depth – RSD: −25 to −40 cm), while at the intermediate position, concentrations peaked at the upper sediment layers (top 20 cm from the sediment surface, RSD: −50 to −70 cm). During the low water stage, concentrations peaked at the lowest depths at the shallow position (around RSD: −50 cm), mid-to-lower depths from the sediment surface at intermediate position (RSD: −80 to −105 cm), and upper sediment layers at the deep position (RSD: −100 to −110 cm). Overall the peaks in methane concentration were observed at upper sediment layers during the falling water stage when the site remained permanently inundated (thick blue line in Fig. 4), and at lower sediment layers during the low water stage when the water level was fluctuating around the reference elevation (thick orange line in Fig. 4).

The peaks may have resulted from a combination of heterotrophic respiration and imports through groundwater into the HZ from the nearby upland area. Methane and CO_2 porewater concentrations were significantly correlated (Fig. 6). Based on the low concentrations of acetate measured in similar sites along the Handford Reach, with only 1/50 samples being above the detection limit (>78 μM), and uncertainty of methyl compound identity and potential utilization (Hou et al., 2017), we infer that the prevailing mode of methanogenesis was hydrogenotrophic, requiring hydrogen and CO_2. However, we acknowledge that this correlation is a function of overall microbial activity, rather than the result of the direct use of CO_2 for methanogenesis alone (Moore and Dalva, 1997; Comer-Warner et al., 2019). Interestingly, we found that the slope of the regression between methane and CO_2 porewater concentrations varied during the three water stages and was larger during the falling water stage when the river downwelling was stronger than during the low water stage when downwelling diminished and groundwater upwelling was more frequent (Fig. 6). The difference in the strength of microbial activity between falling water and low water stages support findings by previous

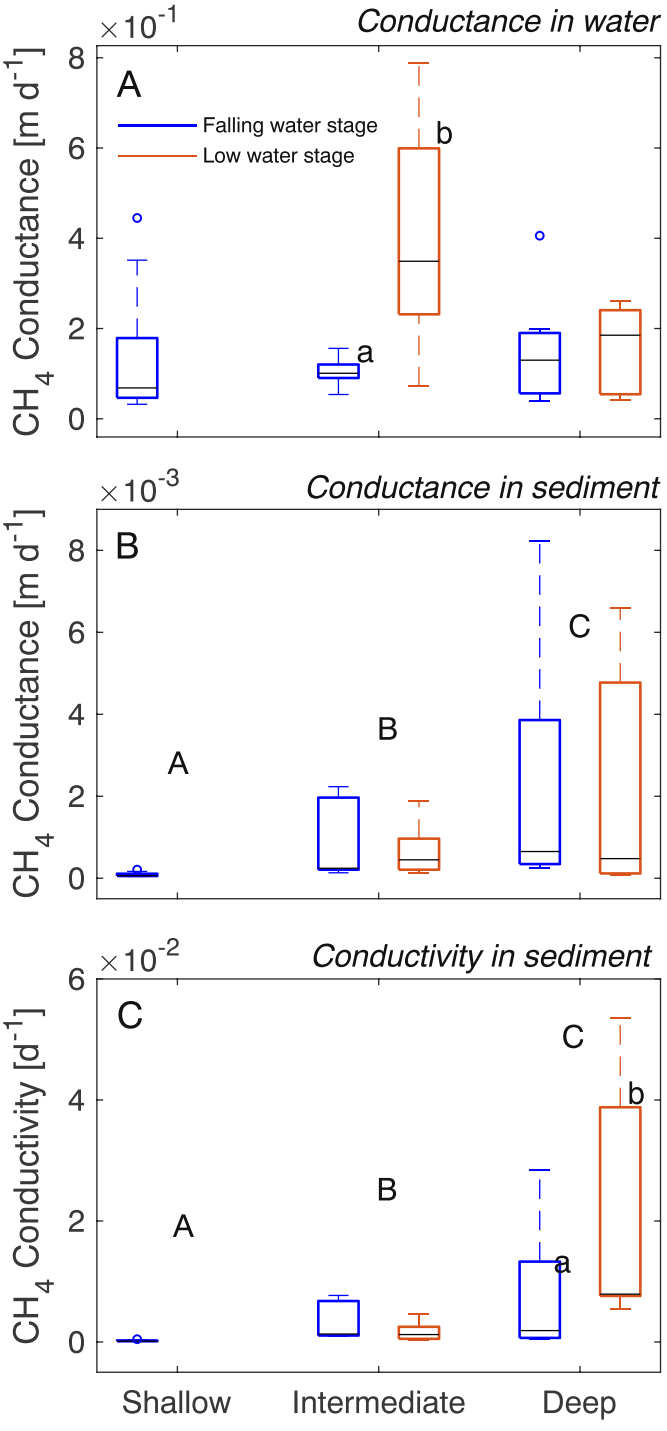

Fig. 5. Methane conductance in the water column and sediments (A and B), and methane conductivity (i.e., conductance per depth) in the sediments (C) along a beach transect (plot scale) at the Columbia River during falling and low river water stages (during the rising water stage fluxes and porewater concentrations were negligible). Boxes represent the 25th and 75th percentiles, the horizontal black line the median and circles outliers defined as observations that are 1.5 greater than the upper interquartile range. Whiskers extend to the furthest observation not considered an outlier. Capital letters indicate differences between beach positions and lowercase letters, differences between river water stages with positions.

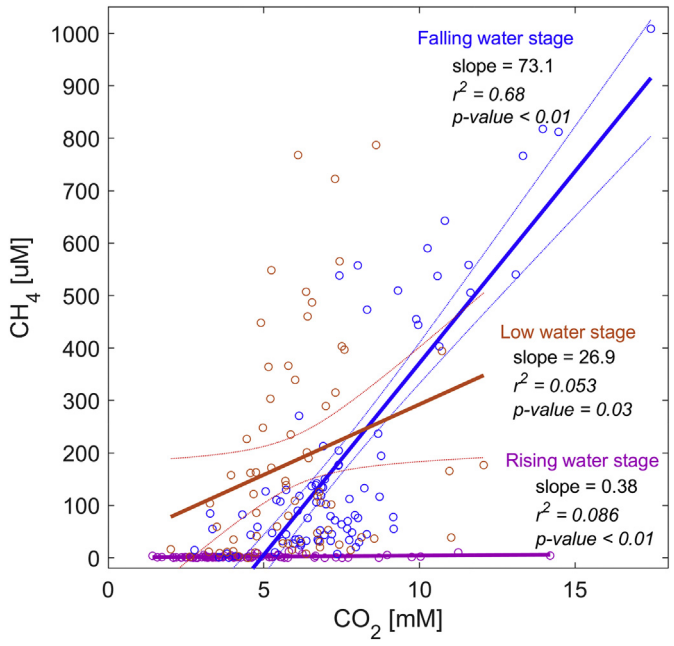

Fig. 6. Correlations between methane and CO_2 porewater concentrations on sediment profiles of a beach transect (plot scale) at the Columbia River during three river water stages. Dotted lines accompanying the regression lines represent the 95% confidence intervals. The correlation is stronger during the falling water stage.

studies at adjacent sites along the Hanford Reach that showed a shift in microbial communities as labile organic carbon stimulates heterotrophic respiration during river downwelling periods (Stegen et al., 2016). As water drops and the influence of groundwater upwelling increases, heterotrophic processes of carbon cycling and decomposition succumb to autotrophic processes (Graham et al., 2017).

On the other hand, as groundwater upwelling becomes more frequent during the low water stage and heterotrophic respiration recede (and presumably the production of methane), imports of dissolved methane in the groundwater increase, maintaining similar porewater concentrations than during the falling water stage. This hypothesis is supported by the increase in conductivity of methane in the sediments we observed at the deep position (Fig. 5C), which indicates that during groundwater upwelling, methane transport is faster. We hypothesize that while microbial methane production is reduced when the water level drops and groundwater upwelling is increased, methane concentrations and fluxes are maintained because allochthonous methane is "pushed out" from the surrounding upland soils and river sediments.

We propose that the observed peaks in methane concentration through the sediment profile during the falling water stage occurred at predominantly anaerobic zones, where hydrological mixing of downwelling surface water from the river and upwelling groundwater from the aquifer is enhanced. The predominant zone of methane production moved vertically downward within the HZ as the river transitioned from falling to low water stage, coinciding with a shift from river water dominated to groundwater-dominated mixing ratios.

3.4. Nitrous oxide porewater concentrations and fluxes have different dynamics across river water stages

Unlike methane, N_2O porewater concentrations in the sediment profile and fluxes to the atmosphere did not follow similar patterns throughout the river water stages (Spearman's $\rho = 0.29$, $p = .14$). N_2O porewater concentrations were higher during the rising water stage than during the falling water stage in all the three beach positions and during the low water stage at the intermediate position (Fig. 7A). Instead, N_2O fluxes increased from the rising to the low water stage at the shallow position, while remained similar at the intermediate and deep positions during the three water stages (Fig. 7B).

The decoupling between the observed N_2O porewater concentrations in the sediments and the fluxes is not surprising. N_2O production in large rivers might occur primarily at the water column in microsites within suspended particles. There is significant evidence of substantial N_2O production via denitrification in pelagic zones of estuaries (Barnes and Owens, 1999; de Wilde and de Bie, 2000). Beaulieu et al. (2010) presented evidence of a similar pattern at a large river, with N_2O production rates in the water column doubling that of the sediments, which could help explain the lack of correlation between the porewater concentrations and fluxes. Marzadri et al. (2014) and Marzadri et al. (2017) explained that in lotic systems there is a shift in the predominant zones of N_2O production from the hyporheic-benthic zone in streams to the benthic-water column zone in rivers as the system gains size, due mainly to the increase in suspended particle loads.

Notably, we observed negative fluxes throughout the different river water stages and in all positions, which is consistent with high rates of N_2O consumption at either the sediments or the water column. Our plot acted primarily as a sink at the shallow position while the

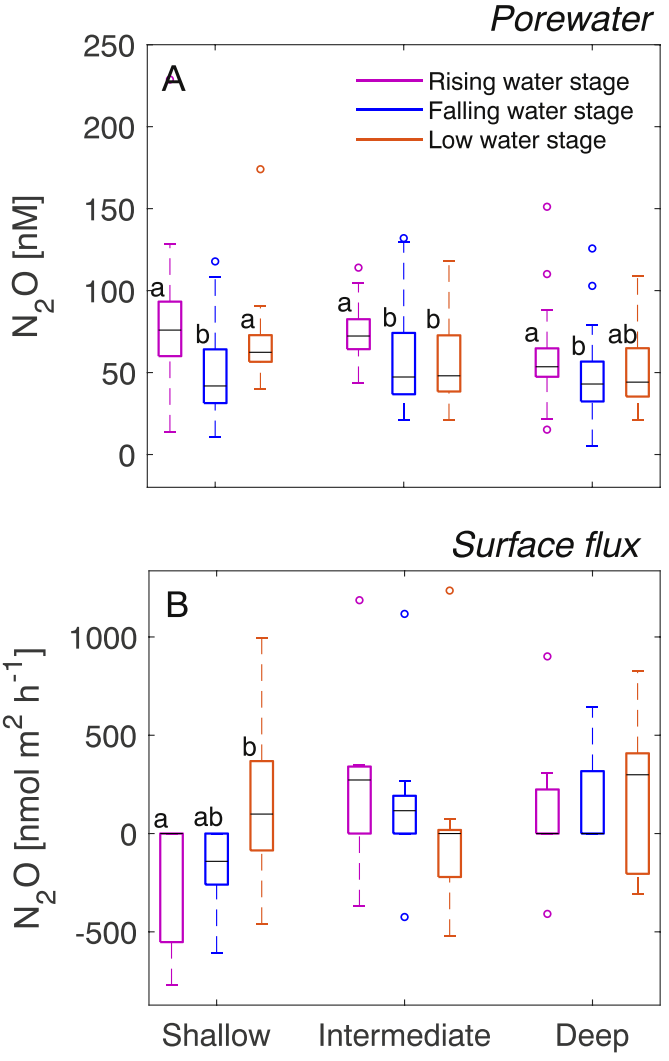

Fig. 7. (A) Integrated sediment-profile methane porewater concentrations and (B) N_2O fluxes along a beach transect (plot scale) at the Columbia River during three river water stages. Boxes represent the 25th and 75th percentiles, the horizontal black line the median and circles outliers defined as observations that are 1.5 greater than the upper interquartile range. Whiskers extend to the furthest observation not considered an outlier. Letters represent statistical differences calculated with non-parametric Wilcoxon paired tests for each position ($\alpha = 0.05$).

sediments were fully saturated, and the water level was above the sediment surface and on the intermediate position during the low water stage when the water level at this position was low as well (Fig. 7A). N_2O is often produced as an intermediate species of microbially mediated denitrification, or a byproduct of nitrification or reduction of ammonia to nitrate (Quick et al., 2019). Dissolved organic carbon in the HZ plays a critical role in fueling nitrification under aerobic conditions (Graham et al., 2016; Graham et al., 2017) and in addition, may lead to low oxygen and nitrate conditions that ultimately favor N_2O consumption (Soued et al., 2015). Low oxygen conditions may result from the low flow as well (Baulch et al., 2011b), which prevailed in the 3G observatory, especially at lower water levels, explaining the dominant sinking functioning of the shallow and intermediate positions partially. It may also be possible that atmospheric nitrous oxide consumption occurred in the water column in the absence of other denitrification processes, which has been demonstrated only for a few model microorganisms and ecosystems (Jones et al., 2014; Yoon et al., 2016).

A more robust understanding of the nexus (or lack thereof) of the spatial heterogeneity and dynamics of N_2O porewater concentrations and fluxes must build upon the synergistic effects of the seasonal hydrological exchanges, inorganic nitrogen availability, and the activity of the microbial community involved in cycling nitrous oxide at the HZ and the water column. For instance, the nitrification and denitrification functional potential of microbial communities in the HZ of the Hanford Reach (and possibly many other lotic systems) are linked with the ratio of groundwater to surface water, likely due to the input of N in the groundwater (Nelson et al., 2019). However, it is still not clear if or how the dynamics of groundwater N or other environmental drivers are affecting the N-cycling functional potential in the water column and overall how N_2O is produced and consumed in the sediment-water column continuum.

3.5. Nitrous oxide concentrations peak at the sediment/water table interface

Mathematical and conceptual models propose that N_2O production at the HZ is maximized along flowlines representing intermediate travel times of downwelling surface water, which are usually few cm below the sediment surface (Reeder et al., 2018; Quick et al., 2016). At shallower depths, at the surface of the sediments (i.e., shortest travel times), nitrate is not transformed, whereas at deeper depths (i.e., longest travel times), denitrification is completed and N_2 is the predominantly released gas. The N_2O porewater concentrations we observed at the 3G are consistent with the modeling predictions, showing increased concentrations at the proximity of the sediment/water table interface (~up to 15 cm) (Fig. 8).

We found significant negative correlations between N_2O and CO_2 porewater concentrations for pooled data from the three water stages and the shallow and intermediate beach positions (Fig. 9). We cannot discern whether the correlation is the result of N_2O production or consumption. Partial denitrification, nitrate reduction to N_2O, is coupled to carbon oxidation to CO_2 and therefore, we would expect a positive

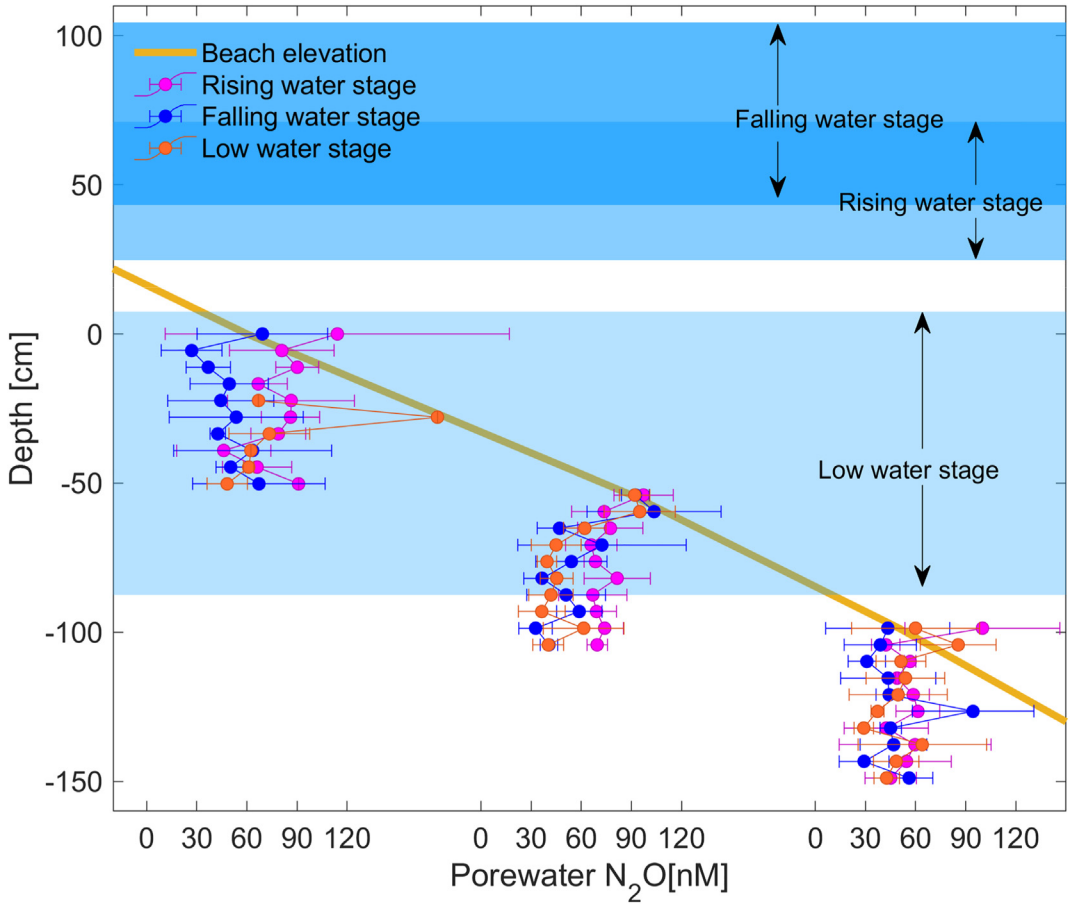

Fig. 8. N_2O porewater concentrations along the sediment profile at shallow (left), intermediate (middle), and deep (right) positions of a beach transect (plot scale) at the Columbia River during three river water stages. Data points (circles) represent the mean concentration, and the error bars the standard error (n = 3). Horizontal blue areas indicate the water level range during the different water stages. The thick brown line represents the beach elevation along the gradient. (For interpretation of the references to color in this figure legend, the reader is referred to the web version of this article.)

correlation (Tsuruta et al., 1997). Therefore, N_2O production appeared decoupled from denitrification and more closely tied to other processes. The negative correlations could be explained by the release of N_2O during nitrification coupled to CO_2 assimilation or heterotrophic microorganisms utilizing N_2O as a terminal electron acceptor (Hink et al., 2017; Lycus et al., 2018). This may help explain the negative correlation between N_2O and CO_2 porewater concentrations, which were also seen in observations of other riverine settings (Richey et al., 1988; Teodoru et al., 2015). However, we do not rule out that simultaneous processes of production and consumption are co-occurring and that their relative importance change as the river water level transitions and substrates, environmental conditions, and the relative diversity and abundance of N-Cycling populations vary (Nelson et al., 2019). The decoupling between N_2O and CO_2 may be explained as well at some degree by lateral transport of N_2O dissolved in groundwater (Clough et al., 2006).

It is noteworthy that the strength of the correlation between N_2O and CO_2 porewater was dictated by beach positions, indicating that different processes are occurring between locations. Weaker negative correlations at the shallow position may be explained by contributions of both nitrification byproducts and denitrification, N_2O consumption as an electron acceptor in the absence of other denitrification processes, and labile carbon oxidation, or the increased contributions from heterotrophic denitrifications. Coupling inorganic nitrogen concentrations and organic carbon concentration measurements should help unveil the prevalence of these processes and their influence in the observed variability between beach positions.

4. Conclusions and outlook

Hyporheic zones of rivers and streams are important hotspots of greenhouse gas emissions. The interaction of river stage and biogeochemical processes govern the production, consumption, and flux dynamics. This interaction of the governing factors results in high heterogeneity at the small scale (m to cm) in horizontal and vertical planes. At the plot scale, methane porewater concentrations have a marked vertical temporal dynamic with concentrations peaking at different depths depending on the influence of the magnitude and direction of hyporheic mixing. Methane fluxes followed the dynamics of porewater concentrations throughout the river water stages but highlighted the potential influence of oxidation in the resulting fluxes. Hence the need for sub-models capable of representing the potential effects of hydrological exchanges on methane oxidation in the HZ. The effect was pronounced for the intermediate position where methane fluxes increased (and the conductance to methane in the water column) from the falling water stage to the low water stage. In turn, N_2O porewater concentrations rely more on the permanent mixing at the HZ and occur at the upper layers just below the sediment surface. Contrary to methane, fluxes of N_2O were not correlated to porewater concentrations and were reduced at low water elevations, possibly because of the release of N_2O as a byproduct of aerobic nitrification or the use of N_2O as an alternative terminal electron acceptor to oxygen for microbial respiration at the sediment-water interface (Khalil et al., 2004; Jones et al., 2014). Overall results indicated that the plot functioned as a net source of methane and could function as either a sink or source for N_2O depending on both the season and position within the riparian zone. Therefore, identifying the potential nexus between N_2O production and consumption and concurrency at the HZ represents a critical challenge for better representation of the N_2O dynamic in biogeochemical models.

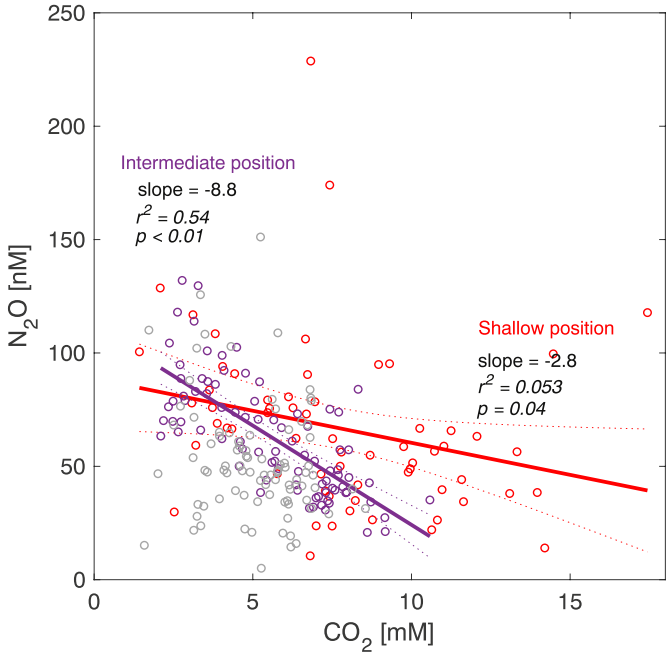

Fig. 9. Correlations between N_2O and CO_2 porewater concentrations along sediment profiles of a beach transect (plot scale) at the Columbia River during three river water stages. Dotted lines accompanying the regression lines represent the 95% confidence intervals. Note that the correlation is not significant for the deep position (gray markers). The overall correlation for data of all positions (not shown) is also significant (slope = −2.97, $r^2 = 0.065$, $p < .01$).

Here we presented snapshots of detailed vertical profiles and surface fluxes of methane and N_2O porewater concentrations through the different typical hydrological stages of a large-regulated river. As our results indicate, river stages and consequent groundwater mixing, drive the dynamics of porewater concentrations and fluxes of methane and N_2O on a seasonal scale. However, coupling hydrological dynamics with methane and N_2O concentrations and fluxes at small scales and parametrizing the governing processes will require longer-term and more frequent assessments, especially the inclusion of measurements at a small temporal scale (days-hours). Such a scale is of particular interest to assess the effects of large intra-daily water level oscillations, which are characteristic of regulated rivers, on the GHG production and consumption processes. This daily/sub-daily measurement scale could help to elucidate the effects of preceding environmental conditions set by previous water levels (including microbial populations, temperature, nutrient availability and transformations, and redox conditions) on the production and consumption of GHGs. In non-regulated rivers, we would expect a similar control of seasonal groundwater mixing than the one we observe here. However, in contrast to regulated rivers, the shorter-term effects of preceding environmental conditions would likely be less dramatic given the lower water intra-daily fluctuations.

Finally, as our results indicate, GHG concentration and fluxes can be significantly different across small horizontal (6 m W × 11 m L) and vertical (0.5 m) spatial scales. Moreover, water level fluctuation has a significant effect on the functioning of the HZ as a sink or source of methane and N_2O. The coupling of hydrology and GHGs emissions at small scales will, therefore, be essential to help parametrize and calibrate predictive models in large rivers like the Columbia River and other rivers and streams as well. More importantly, it is a necessary task to test hypotheses discerning the microbial processes explaining the spatiotemporal heterogeneity of methane and N_2O at the HZ.

Declaration of competing interest

The authors declare that they have no known competing financial interests or personal relationships that could have appeared to influence the work reported in this paper.

Acknowledgments

This project was sponsored by the Subsurface Biogeochemical Research (SBR) program (DE-SC0018170).

References

Anthony, S.E., Prahl, F.G., Peterson, T.D., 2012. Methane dynamics in the Willamette River, Oregon. Limnol. Oceanogr. 57, 1517–1530. https://doi.org/10.4319/lo.2012.57.5.1517.

Aufdenkampe, A.K., Mayorga, E., Raymond, P.A., Melack, J.M., Doney, S.C., Alin, S.R., Aalto, R.E., Yoo, K., 2011. Riverine coupling of biogeochemical cycles between land, oceans, and atmosphere. Front. Ecol. Environ. 9, 53–60. https://doi.org/10.1890/100014.

Barnes, J., Owens, N.J.P., 1999. Denitrification and nitrous oxide concentrations in the Humber estuary, UK, and adjacent coastal zones. Mar. Pollut. Bull. 37, 247–260. https://doi.org/10.1016/S0025-326X(99)00079-X.

Bastviken, D., Cole, J., Pace, M., Tranvik, L., 2004. Methane emissions from lakes: dependence of lake characteristics, two regional assessments, and a global estimate. Glob. Biogeochem. Cycles 18, GB4009. https://doi.org/10.1029/2004GB002238.

Baulch, H.M., Dillon, P.J., Maranger, R., Schiff, S.L., 2011a. Diffusive and ebullitive transport of methane and nitrous oxide from streams: are bubble-mediated fluxes important? J. Geophys. Res. Biogeosci. 116. https://doi.org/10.1029/2011JG001656.

Baulch, H.M., Schiff, S.L., Maranger, R., Dillon, P.J., 2011b. Nitrogen enrichment and the emission of nitrous oxide from streams. Glob. Biogeochem. Cycles 25, GB4013. https://doi.org/10.1029/2011GB004047.

Beaulieu, J.J., Shuster, W.D., Rebholz, J.A., 2010. Nitrous oxide emissions from a large, impounded river: the Ohio River. Environ. Sci. Technol. 44, 7527–7533. https://doi.org/10.1021/es1016735.

Beaulieu, J.J., Tank, J.L., Hamilton, S.K., Wollheim, W.M., Hall, R.O., Mulholland, P.J., Peterson, B.J., Ashkenas, L.R., Cooper, L.W., Dahm, C.N., Dodds, W.K., Grimm, N.B., Johnson, S.L., McDowell, W.H., Poole, G.C., Valett, H.M., Arango, C.P., Bernot, M.J., Burgin, A.J., Crenshaw, C.L., Helton, A.M., Johnson, L.T., O'Brien, J.M., Potter, J.D., Sheibley, R.W., Sobota, D.J., Thomas, S.M., 2011. Nitrous oxide emission from denitrification in stream and river networks. Proc. Natl. Acad. Sci. 108, 214. https://doi.org/10.1073/pnas.1011464108.

Bednařík, A., Čáp, L., Maier, V., Rulík, M., 2015. Contribution of methane benthic and atmospheric fluxes of an experimental area (Sitka Stream). CLEAN – Soil Air Water 43, 1136–1142. https://doi.org/10.1002/clen.201300982.

Bethke, C.M., Sanford, R.A., Kirk, M.F., Jin, Q., Flynn, T.M., 2011. The thermodynamic ladder in geomicrobiology. Am. J. Sci. 311, 183–210. https://doi.org/10.2475/03.2011.01.

Boulton, A.J., Findlay, S., Marmonier, P., Stanley, E.H., Valett, H.M., 1998. The functional significance of the hyporheic zone in streams and rivers. Annu. Rev. Ecol. Syst. 29, 59–81. https://doi.org/10.1146/annurev.ecolsys.29.1.59.

Bridgham, S.D., Cadillo-Quiroz, H., Keller, J.K., Zhuang, Q., 2013. Methane emissions from wetlands: biogeochemical, microbial, and modeling perspectives from local to global scales. Glob. Change Biol. 19, 1325–1346. https://doi.org/10.1111/gcb.12131.

Buchkowski, R.W., Bradford, M.A., Grandy, A.S., Schmitz, O.J., Wieder, W.R., 2017. Applying population and community ecology theory to advance understanding of belowground biogeochemistry. Ecol. Lett. 20, 231–245. https://doi.org/10.1111/ele.12712.

Chistoserdova, L., Kalyuzhnaya, M.G., Lidstrom, M.E., 2009. The expanding world of methylotrophic metabolism. Annu. Rev. Microbiol. 63, 477–499. https://doi.org/10.1146/annurev.micro.091208.073600.

Clough, T.J., Bertram, J.E., Sherlock, R.R., Leonard, R.L., Nowicki, B.L., 2006. Comparison of measured and EF5-r-derived N_2O fluxes from a spring-fed river. Glob. Chang. Biol. 12, 477–488. https://doi.org/10.1111/j.1365-2486.2005.01092.x.

Cole, J., Prairie, Y., Caraco, N., McDowell, W., Tranvik, L., Striegl, R., Duarte, C., Kortelainen, P., Downing, J., Middelburg, J., Melack, J., 2007. Plumbing the global carbon cycle: integrating inland waters into the terrestrial carbon budget. Ecosystems 10, 172–185.

Comer-Warner, S.A., Romeijn, P., Gooddy, D.C., Ullah, S., Kettridge, N., Marchant, B., Hannah, D.M., Krause, S., 2018. Thermal sensitivity of CO_2 and CH_4 emissions varies with streambed sediment properties. Nat. Commun. 9, 2803. https://doi.org/10.1038/s41467-018-04756-x.

Comer-Warner, S.A., Gooddy, D.C., Ullah, S., Glover, L., Percival, A., Kettridge, N., Krause, S., 2019. Seasonal variability of sediment controls of carbon cycling in an agricultural stream. Sci. Total Environ. 688, 732–741. https://doi.org/10.1016/j.scitotenv.2019.06.317.

Conrad, R., Rothfuss, F., 1991. Methane oxidation in the soil surface layer of a flooded rice field and the effect of ammonium. Biol. Fertil. Soils 12, 28–32. https://doi.org/10.1007/BF00369384.

Golaz, J., Caldwell, P.M., Van Roekel, L.P., Petersen, M.R., Tang, Q., Wolfe, J.D., Abeshu, G., Anantharaj, V., Asay-Davis, X.S., Bader, D.C., 2019. The DOE E3SM coupled model version 1: overview and evaluation at standard resolution. J. Adv. Model. Earth Syst. 11, 2089–2129.

Graham, E.B., Crump, A.R., Resch, C.T., Fansler, S., Arntzen, E., Kennedy, D.W., Fredrickson, J.K., Stegen, J.C., 2016. Coupling spatiotemporal community assembly processes to changes in microbial metabolism. Front. Microbiol. 7, 1949. https://doi.org/10.3389/fmicb.2016.01949.

Graham, E.B., Crump, A.R., Resch, C.T., Fansler, S., Arntzen, E., Kennedy, D.W., Fredrickson, J.K., Stegen, J.C., 2017. Deterministic influences exceed dispersal effects on hydrologically-connected microbiomes. Environ. Microbiol. 19, 1552–1567. https://doi.org/10.1111/1462-2920.13720.

Graham, E.B., Stegen, J.C., Huang, M., Chen, X., Scheibe, T.D., 2019. Subsurface biogeochemistry is a missing link between ecology and hydrology in dam-impacted river corridors. Sci. Total Environ. 657, 435–445. https://doi.org/10.1016/j.scitotenv.2018.11.414.

Hink, L., Lycus, P., Gubry-Rangin, C., Frostegård, Å., Nicol, G.W., Prosser, J.I., Bakken, L.R., 2017. Kinetics of NH3-oxidation, NO-turnover, N_2O-production and electron flow during oxygen depletion in model bacterial and archaeal ammonia oxidisers. Environ. Microbiol. 19, 4882–4896. https://doi.org/10.1111/1462-2920.13914.

Holland, E.A., Robertson, G.P., Greenberg, J., Groffman, P.M., Boone, R.D., Grosz, J.R., 1999. Soil CO_2,N_2O and CH_4 exchange. Standard Soil Methods for Long-Term Ecological Research. Oxford University Press, New York, pp. 185–201.

Hotchkiss, E.R., Hall Jr, R.O., Sponseller, R.A., Butman, D., Klaminder, J., Laudon, H., Rosvall, M., Karlsson, J., 2015. Sources of and processes controlling CO_2 emissions change with the size of streams and rivers. Nat. Geosci. 8, 696.

Hou, Z., Nelson, W.C., Stegen, J.C., Murray, C.J., Arntzen, E., Crump, A.R., Kennedy, D.W., Perkins, M.C., Scheibe, T.D., Fredrickson, J.K., Zachara, J.M., 2017. Geochemical and microbial community attributes in relation to hyporheic zone geological facies. Sci. Rep. 7, 12006. https://doi.org/10.1038/s41598-017-12275-w.

Hutchinson, G., Mosier, A., 1981. Improved soil cover method for field measurement of nitrous oxide fluxes 1. Soil Sci. Soc. Am. J. 45, 311–316.

Jackson, R.B., Le Quéré, C., Andrew, R.M., Canadell, J.G., Peters, G.P., Roy, J., Wu, L., 2017. Warning signs for stabilizing global CO_2 emissions. Environ. Res. Lett. 12, 110202. https://doi.org/10.1088/1748-9326/aa9662.

Jones, J.B., Mulholland, P.J., 1998. Influence of drainage basin topography and elevation on carbon dioxide and methane supersaturation of stream water. Biogeochemistry 40, 57–72.

Jones, C.M., Spor, A., Brennan, F.P., Breuil, M.-C., Bru, D., Lemanceau, P., Griffiths, B., Hallin, S., Philippot, L., 2014. Recently identified microbial guild mediates soil N_2O sink capacity. Nat. Clim. Chang. 4, 801.

Joulian, C., Escoffier, S., Le Mer, J., Neue, H., Roger, P.-A., 1997. Populations and potential activities of methanogens and methanotrophs in rice fields: relations with soil properties. Eur. J. Soil Biol. 33, 105–116.

Kampbell, D.H., Wilson, J.T., Vandegrift, S.A., 1989. Dissolved oxygen and methane in water by a GC headspace equilibration technique. Int. J. Environ. Anal. Chem. 36, 249–257. https://doi.org/10.1080/03067319808026878.

Khalil, K., Mary, B., Renault, P., 2004. Nitrous oxide production by nitrification and denitrification in soil aggregates as affected by O_2 concentration. Soil Biol. Biochem. 36, 687–699. https://doi.org/10.1016/j.soilbio.2004.01.004.

Krause, S., Hannah, D.M., Fleckenstein, J.H., Heppell, C.M., Kaeser, D., Pickup, R., Pinay, G., Robertson, A.L., Wood, P.J., 2011. Inter-disciplinary perspectives on processes in the hyporheic zone. Ecohydrology 4, 481–499. https://doi.org/10.1002/eco.176.

Kutzbach, L., Scneider, J., Sachs, T., Giebels, M., Nykänen, H., Shurpali, N.J., Martikainen, P.J., Alm, J., Wilmking, M., 2007. CO_2 flux determination by closed-chamber methods can be seriously biased by inappropriate application of linear regression. Biogeosciences 4, 1005–1025.

Le Mer, J., Roger, P., 2001. Production, oxidation, emission and consumption of methane by soils: a review. Eur. J. Soil Biol. 37, 25–50. https://doi.org/10.1016/S1164-5563(01)01067-6.

Lei, D., Liu, J., Zhang, J., Lorke, A., Xiao, S., Wang, Y., Wang, W., Li, Y., 2019. Methane oxidation in the water column of Xiangxi Bay, Three Gorges Reservoir. CLEAN – Soil Air Water 47, 1800516. https://doi.org/10.1002/clen.201800516.

Lycus, P., Soriano-Laguna, M.J., Kjos, M., Richardson, D.J., Gates, A.J., Milligan, D.A., Frostegård, Å., Bergaust, L., Bakken, L.R., 2018. A bet-hedging strategy for denitrifying bacteria curtails their release of N_2O. Proc. Natl. Acad. Sci. 115, 11820. https://doi.org/10.1073/pnas.1805000115.

Lyu, Z., Shao, N., Akinyemi, T., Whitman, W.B., 2018. Methanogenesis. Curr. Biol. 28, R727–R732. https://doi.org/10.1016/j.cub.2018.05.021.

MacDonald, L.H., Paull, J.S., Jaffé, P.R., 2013. Enhanced semipermanent dialysis samplers for long-term environmental monitoring in saturated sediments. Environ. Monit. Assess. 185, 3613–3624. https://doi.org/10.1007/s10661-012-2813-8.

Marzadri, A., Tonina, D., Bellin, A., Tank, J.L., 2014. A hydrologic model demonstrates nitrous oxide emissions depend on streambed morphology. Geophys. Res. Lett. 41, 5484–5491. https://doi.org/10.1002/2014GL060732.

Marzadri, A., Dee, M.M., Tonina, D., Bellin, A., Tank, J.L., 2017. Role of surface and subsurface processes in scaling N_2O emissions along riverine networks. Proc. Natl. Acad. Sci. 114, 4330. https://doi.org/10.1073/pnas.1617454114.

Matoušů, A., Osudar, R., Šimek, K., Bussmann, I., 2017. Methane distribution and methane oxidation in the water column of the Elbe estuary, Germany. Aquat. Sci. 79, 443–458. https://doi.org/10.1007/s00027-016-0509-9.

Matoušů, A., Rulík, M., Tušer, M., Bednařík, A., Šimek, K., Bussmann, I., 2018. Methane dynamics in a large river: a case study of the Elbe River. Aquat. Sci. 81, 12. https://doi.org/10.1007/s00027-018-0609-9.

McClain, M.E., Boyer, E.W., Dent, C.L., Gergel, S.E., Grimm, N.B., Groffman, P.M., Hart, S.C., Harvey, J.W., Johnston, C.A., Mayorga, E., McDowell, W.H., Pinay, G., 2003. Biogeochemical hot spots and hot moments at the interface of terrestrial and aquatic ecosystems. Ecosystems 6, 301–312. https://doi.org/10.1007/s10021-003-0161-9.

Moore, T.R., Dalva, M., 1997. Methane and carbon dioxide exchange potentials of peat soils in aerobic and anaerobic laboratory incubations. Soil Biol. Biochem. 29, 1157–1164. https://doi.org/10.1016/S0038-0717(97)00037-0.

Nelson, W.C., Graham, E.B., Crump, A.R., Fansler, S.J., Arntzen, E.V., Kennedy, D.W., Stegen, J.C., 2019. Temporal Dynamics of Nitrogen Cycle Gene Diversity in a Hyporheic Microbiome. bioRxiv 722785. https://doi.org/10.1101/722785.

Neubauer, ScottC, Megonigal, J.P., 2015. Moving beyond global warming potentials to quantify the climatic role of ecosystems. Ecosystems 18, 1000–1013. https://doi.org/10.1007/s10021-015-9879-4.

Oremland, R.S., Culbertson, C.W., 1992. Importance of methane-oxidizing bacteria in the methane budget as revealed by the use of a specific inhibitor. Nature 356, 421–423. https://doi.org/10.1038/356421a0.

Pedersen, A.R., Petersen, S.O., Schelde, K., 2010. A comprehensive approach to soil-atmosphere trace-gas flux estimation with static chambers. Eur. J. Soil Sci. 61, 888–902. https://doi.org/10.1111/j.1365-2389.2010.01291.x.

Quick, A.M., Reeder, W.J., Farrell, T.B., Tonina, D., Feris, K.P., Benner, S.G., 2016. Controls on nitrous oxide emissions from the hyporheic zones of streams. Environ. Sci. Technol. 50, 11491–11500. https://doi.org/10.1021/acs.est.6b02680.

Quick, A.M., Reeder, W.J., Farrell, T.B., Tonina, D., Feris, K.P., Benner, S.G., 2019. Nitrous oxide from streams and rivers: a review of primary biogeochemical pathways and environmental variables. Earth-Sci. Rev. 191, 224–262. https://doi.org/10.1016/j.earscirev.2019.02.021.

Raymond, P.A., Hartmann, J., Lauerwald, R., Sobek, S., McDonald, C., Hoover, M., Butman, D., Striegl, R., Mayorga, E., Humborg, C., Kortelainen, P., Dürr, H., Meybeck, M., Ciais, P., Guth, P., 2013. Global carbon dioxide emissions from inland waters. Nature 503, 355–359. https://doi.org/10.1038/nature12760.

Reeder, W.J., Quick, A.M., Farrell, T.B., Benner, S.G., Feris, K.P., Marzadri, A., Tonina, D., 2018. Hyporheic source and sink of nitrous oxide. Water Resour. Res. 54, 5001–5016. https://doi.org/10.1029/2018WR022564.

Rey-Sanchez, A.C., Morin, T.H., Stefanik, K.C., Wrighton, K., Bohrer, G., 2018. Determining total emissions and environmental drivers of methane flux in a Lake Erie estuarine marsh. Ecol. Eng. 114, 7–15. https://doi.org/10.1016/j.ecoleng.2017.06.042.

Rey-Sanchez, C., Bohrer, G., Slater, J., Li, Y.-F., Grau-Andrés, R., Hao, Y., Rich, V.I., Davies, G.M., 2019. The ratio of methanogens to methanotrophs and water-level dynamics drive methane transfer velocity in a temperate kettle-hole peat bog. Biogeosciences 16, 3207–3231. https://doi.org/10.5194/bg-16-3207-2019.

Richey, J.E., Devol, A.H., Wofsy, S.C., Victoria, R., Riberio, M.N.G., 1988. Biogenic gases and the oxidation and reduction of carbon in Amazon River and floodplain waters. Limnol. Oceanogr. 33, 551–561. https://doi.org/10.4319/lo.1988.33.4.0551.

Romeijn, P., Comer-Warner, S.A., Ullah, S., Hannah, D.M., Krause, S., 2019. Streambed organic matter controls on carbon dioxide and methane emissions from streams. Environ. Sci. Technol. 53, 2364–2374. https://doi.org/10.1021/acs.est.8b04243.

Rulík, M., Čáp, L., Hlaváčová, E., 2000. Methane in the hyporheic zone of a small lowland stream (Sitka, Czech Republic). Limnologica 30, 359–366. https://doi.org/10.1016/S0075-9511(00)80029-8.

Saunois, M., Bousquet, P., Poulter, B., Peregon, A., Ciais, P., Canadell, J.G., Dlugokencky, E.J., Etiope, G., Bastviken, D., Houweling, S., 2016. The global methane budget 2000–2012. Earth Syst. Sci. Data 8, 697–751.

Schindler, J.E., 1998. The hyporheic zone as a source of dissolved organic carbon and carbon gases to a temperate forested stream. Biogeochemistry 43, 157–174.

Segers, R., 1998. Methane production and methane consumption: a review of processes underlying wetland methane fluxes. Biogeochemistry 41, 23–51. https://doi.org/10.1023/A:1005929032764.

Soued, C., del Giorgio, P.A., Maranger, R., 2015. Nitrous oxide sinks and emissions in boreal aquatic networks in Québec. Nat. Geosci. 9, 116.

Stanley, E.H., Casson, N.J., Christel, S.T., Crawford, J.T., Loken, L.C., Oliver, S.K., 2016. The ecology of methane in streams and rivers: patterns, controls, and global significance. Ecol. Monogr. 86, 146–171.

Stegen, J.C., Fredrickson, J.K., Wilkins, M.J., Konopka, A.E., Nelson, W.C., Arntzen, E.V., Chrisler, W.B., Chu, R.K., Danczak, R.E., Fansler, S.J., Kennedy, D.W., Resch, C.T., Tfaily, M., 2016. Groundwater–surface water mixing shifts ecological assembly processes and stimulates organic carbon turnover. Nat. Commun. 7, 11237. https://doi.org/10.1038/ncomms11237.

Teodoru, C.R., Nyoni, F.C., Borges, A.V., Darchambeau, F., Nyambe, I., Bouillon, S., 2015. Dynamics of greenhouse gases (CO_2, CH_4, N_2O) along the Zambezi River and major tributaries, and their importance in the riverine carbon budget. Biogeosciences 12, 2431–2453. https://doi.org/10.5194/bg-12-2431-2015.

Tsuruta, H., Kanda, K., Hirose, T., 1997. Nitrous oxide emission from a rice paddy field in Japan. Nutr. Cycl. Agroecosystems 49, 51–58. https://doi.org/10.1023/A:1009739830004.

Valentine, D.L., Blanton, D.C., Reeburgh, W.S., Kastner, M., 2001. Water column methane oxidation adjacent to an area of active hydrate dissociation, Eel river Basin. Geochim. Cosmochim. Acta 65, 2633–2640. https://doi.org/10.1016/S0016-7037(01)00625-1.

de Wilde, H.P.J., de Bie, M.J.M., 2000. Nitrous oxide in the Schelde estuary: production by nitrification and emission to the atmosphere. Mar. Chem. 69, 203–216. https://doi.org/10.1016/S0304-4203(99)00106-1.

Woessner, W.W., 2017. Chapter 8 - hyporheic zones. In: Hauer, F.R., Lamberti, G.A. (Eds.), Methods in Stream Ecology, Third edition Vol. 1. Academic Press, Boston, pp. 129–157. https://doi.org/10.1016/B978-0-12-416558-8.00008-1.

Yoon, S., Nissen, S., Park, D., Sanford, R.A., Löffler, F.E., 2016. Nitrous oxide reduction kinetics distinguish bacteria harboring Clade I NosZ from those harboring Clade II NosZ. Appl. Environ. Microbiol. 82, 3793–3800. https://doi.org/10.1128/AEM.00409-16.

Yvon-Durocher, G., Allen, A.P., Bastviken, D., Conrad, R., Gudasz, C., St-Pierre, A., Thanh-Duc, N., del Giorgio, P.A., 2014. Methane fluxes show consistent temperature dependence across microbial to ecosystem scales. Nature 507, 488.

Zhou, T., Bao, J., Huang, M., Hou, Z., Arntzen, E., Song, X., Harding, S.F., Titzler, P.S., Ren, H., Murray, C.J., Perkins, W.A., Chen, X., Stegen, J.C., Hammond, G.E., Thorne, P.D., Zachara, J.M., 2018. Riverbed hydrologic exchange dynamics in a large regulated river reach. Water Resour. Res. 54, 2715–2730. https://doi.org/10.1002/2017WR020508.

Zhu, C., Talbot, H.M., Wagner, T., Pan, J.M., Pancost, R.D., 2010. Intense aerobic methane oxidation in the Yangtze Estuary: a record from 35-aminobacteriohopanepolyols in surface sediments. Adv. Org. Geochem. 2009 (41), 1056–1059. https://doi.org/10.1016/j.orggeochem.2010.03.015.